Chromatographic Fractionation of SWNT/DNA Dispersions with On-Line Multi-Angle Light Scattering

Barry J. Bauer,* Jeffrey A. Fagan, Erik K. Hobbie, Jaehun Chun, and Vardhan Bajpai

National Institute of Standards and Technology, Polymers Division, Gaithersburg, Maryland 20899

Received: September 13, 2007; In Final Form: November 6, 2007

Single wall carbon nanotubes (SWNTs) dispersed in aqueous medium by the use of DNA are separated by size using a size exclusion chromatographic (SEC) column. On-line measurements are made of SWNT concentration, molar mass, and size using UV−vis absorption detection and multi-angle light scattering (MALS). Molar mass and length distributions are calculated for SWNT dispersions from this data. The SWNTs are shown to separate primarily by a SEC mechanism, but the elution times are affected by a high performance liquid chromatography (HPLC) mechanism in which adsorption on the column delays the elution of the components. This mechanism is most evident by the elution of small quantities of large, polydisperse SWNTs after the SEC column limit. MALS data are fit with a polydisperse anisotropic rod scattering function giving low polydispersity for most of the fractions with higher polydispersities near the large size exclusion limit and beyond the small size exclusion limit of the SEC column. These fits indicate that molar mass is proportional to the rod length over a wide range indicating rigid-rod behavior.

Introduction

Single wall carbon nanotubes (SWNTs) have a variety of potential applications in materials because of their outstanding mechanical, electrical, optical, and thermal properties.[1] However, as produced, SWNTs contain bundles of nanotubes comprised of tubes with a distribution of lengths, chiralities, and diameters that are often contaminated with non-SWNT carbon. Such mixtures are unsuitable for most applications and characterization methods without further processing.[2,3] Methods are thus required to sort nanotubes by size and type as well as to eliminate combinations of different nanotubes (bundles) and carbonaceous impurities. Only after purification and sorting can measurements be made of properties inherent to individual SWNTs with low polydispersities. SWNTs have two primary forms of polydispersity, type (chirality and diameter) and length. Sorting by length is the topic of this manuscript, but many efforts are underway for sorting by type.[4−10] Another important goal is to develop an analytical method of determining the molar mass and size distributions of polydisperse SWNTs.

Several methods of producing varied sizes of SWNTs dispersed in liquids have been reported: field flow fractionation (FFF),[11−14] chemical or physical SWNT fracture,[3,4,12,15−19] and size exclusion chromatography (SEC).[20−26] FFF is a commonly used method of separating dissolved polymers or dispersed nanoparticles.[27] Separations of SWNTs by FFF have been reported for aqueous dispersions using surfactants as dispersants. Although FFF is a promising technique with a potential for strong size resolution, the capacity to produce sizable quantities of fractionated samples via this method has not been demonstrated. Significant quantities of different average length SWNTs can be generated by breaking the as-produced nanotubes through treatment with concentrated acids,[12,17−19] long sonication times,[3,4] or mechanical milling.[15,16] Microscopy shows decreased average lengths with processing time, but polydispersity in the lengths

and general degradation of the starting material is expected for such random breakdown.

SEC in contrast is a routine and scalable separation method for polymeric materials and has been applied to the case of nanotube dispersions. In SEC, a porous column packing material is used to separate dissolved polymer molecules by size. The polymers partition between the flowing mobile phase and the stationary phase, which is incorporated within the pores of the column packing material. The smaller polymers have a greater partitioning coefficient inside of the pores than the larger ones. This results in the larger polymers spending a greater fraction of time in the flowing mobile phase, hence, eluting from the column before the smaller ones.[28] The partitioning of the polymers will depend on the characteristic volume of the polymers, which is commonly associated with their hydrodynamic volume. Universal calibration[28] is a technique that assumes that elution time is a function of the hydrodynamic volume alone and, therefore, allows a column set to be calibrated with a set of polymers having known hydrodynamic volumes. With this calibration, the column set can then be used to measure other polymers or nanoparticles with unknown sizes and shapes.

SEC is most commonly run with "good" solvents that have favorable thermodynamic interactions with the solute. "Poor" solvents are avoided not only to avoid aggregation or ultimately precipitation of the solute, but also to inhibit any interactions of the solute with the column packing material. High performance liquid chromatography (HPLC) is a separation technique that also uses porous, high surface area column packing material, but the separations are driven by favorable thermodynamic interactions with the pore surface rather than the pore void volumes. A partitioning is established between adsorption on the surface and suspension in the flowing liquid causing solute with favorable interactions to spend more time in the "stationary" phase and hence elute later. The HPLC mechanism causes large molecules to elute later than small molecules of the same type. The combination of SEC and HPLC mechanisms has been used to minimize the separation by size and emphasize the

separation by other factors such as end-group type.[29] However, if the ultimate goal is to separate by size, the HPLC mechanism is inhibited by choice of solvents having a strong interaction with the solute.

SEC has been reported for a variety of SWNT dispersions using surfactants, wrapping polymers, and covalent modification.[20,22−26,30] Size separation and dispersion quality are commonly measured through atomic force microscopy (AFM), but small angle neutron scattering and viscosity detection has also been reported. Of the multitude of dispersion schemes reported, dispersions with DNA seem to be the prime candidate for liquid separations. The chief traits of DNA dispersions are that a large majority of SWNTs are dispersed as individuals even for relatively high concentrations (up to approximately 0.8 mg/mL). This is true even after excess DNA is removed from the SWNT solution, as occurs in the SEC process. These traits are important because separation of SWNTs by size or type requires that they are unattached to other nanotubes as in the case of SWNT bundles, so good dispersion is a prerequisite. Therefore, we have chosen the method of Zheng et al.,[25] which has previously been demonstrated to produce these important traits, and to disperse our SWNTs with 30-mer 5′-GT(GT)$_{13}$GT-3′ single stranded DNA.

Multi-angle light scattering (MALS) is capable of measuring important information on the size and shape of nanoparticles. It has a long history of measurements made on liquid dispersions, both on flexible polymeric chains dissolved in solvent and on small objects such as latex particles dispersed in aqueous media. MALS has been reported[31−33] on SWNT/DNA dispersions on individual samples and power law scattering differentiates clusters from well-dispersed rod-like SWNTs. However, on-line measurements of chromatographic fractions have not been reported in the literature to our knowledge. We have developed a method of measuring the molar mass and size distributions of SWNTs in quick, reliable way. SEC with on-line MALS is used for both analytical determination of SWNT populations and preparative collection of samples for a variety of off-line measurements.[34,35]

Experimental Section

The measurements presented here were performed on SWNTs grown through the cobalt-molybdenum-catalyst (CoMoCAT) process, but analogous behavior was also measured for SWNTs grown with HiPco, laser ablation, and electric arc methods. Aqueous dispersions of CoMoCAT SWNTs (Southwest Nanotechnologies Inc. Batch NI-6-A001 S-P95-02) were achieved following the method of Zheng et al.[25] by sonication in an ice water bath (10 W, 3.2 mm tip sonicator) of 1 mg/mL SWNTs in salt solution (0.2 mol/L NaCl, 0.04 mol/L Tris, HCl to pH = 7.0) in the presence of 1 mg/mL 30-mer 5′-GT(GT)$_{13}$GT-3′ single stranded DNA (Integrated DNA Technologies) for 2 h, followed by centrifugation (2 h, 21 000 × g). The supernatant was a stable black liquid that has been shown to contain well-dispersed SWNTs. Upon centrifugation, residual catalyst was reduced to <1% by mass as determined by X-ray photoemission spectroscopy, and carbon content of the SWNT was greater than 90% by mass of SWNTs indicated.[34,36,37]

SEC was performed using an Agilent 1200 pump with a SepaxCNT (SEC-2000 + SEC-1000 + SEC-300) column set. The mobile phase used was identical to that of the salt solution used to suspend the samples (0.2 mol/L NaCl, 0.04 mol/L Tris, HCl to pH = 7.0) as has been previously described.[26] No additional DNA was used in the mobile phase. Centrifuged samples were filtered through a 0.45 µm filter and injected in

0.5 mL increments with a 0.5 mL/min flow rate. For samples used in this contribution, very little material was seen to remain on the filter after the filtration step. Thirty fractions were collected at 2 min intervals spanning the time range from before the maximum size exclusion limit to beyond the minimum size exclusion limit "trash peak". Eight repetitions of the chromatographic separation were performed for the SWNT/DNA. For all runs of chromatographic separation, a UV−vis absorbance detector (Waters 2487) was used for concentration detection and a UV−vis photodiode array (Waters 2996) was used to record the absorbance spectrum (200 to 800 nm) as a function of time. Measurements of biotoxcity[34] and length dependent optical properties[37] have been reported on fractions prepared in our laboratory by this method.

The MALS data were taken with a Wyatt Dawn EOS instrument with a flow-through cell capable of recording scattered light intensity at 16 angles. Fluorescence interference was eliminated by use of filters over alternating detectors, and seven of the detectors were used for data analysis incorporating the whole available angular range. A forward laser monitor was used to measure the absorption of the 690 nm incident beam. Astra Software was used to collect the MALS and UV−vis absorbance and to correct for laser absorption at the scattering volume. Absolute scattering intensity was calculated from Rayleigh scattering from toluene and MALS detector sensitivity was calibrated with a narrow poly(methacrylic acid) standard. The data were output and fit as described in a later section.

SWNT extinction coefficient was measured with a Perkin-Elmer Lambda 950 UV−vis-NIR spectrophotometer. UV−visible (vis)-NIR absorption spectroscopy was performed in transmission mode over the range of 1880 to 185 nm. Samples of a known mass were prepared as described above and a spectrum was taken before centrifugation to ensure that the concentration was unchanged from the concentrations calculated from the masses present. Absorption at 690 nm was used to calculate the concentration, c, and an extinction coefficient of $\epsilon = 26\,000$ cm^2/g was used in the calculations, $AU = -\log(I/I_0) = \epsilon t c$, where t is the path length, and I/I_0 is the transmission. The relative uncertainty is estimated to be 10% because of the compositional effects, described elsewhere.[37]

Refractive index increment, dn/dc, was measured at 690 nm with a Wyatt Optilab rEX refractometer on samples prepared as described above and is described in Supporting Information. The instrument utilizes a photodiode array to measure beam deflection directly and is unaffected by absorption effects. The light source has $\lambda_0 = 690$ nm that is the same as the MALS wavelength but is from a light emitting diode and is unpolarized. The concentration was monitored by absorption at 690 nm as described above, and Astra software was used to calculate dn/dc. A value of (0.373 ± 0.013) mL/g was calculated from a linear least-squares fit and is described in Supporting Information. Such measurements are appropriate for isotropic polymers that make up a large majority of MALS samples. However, anisotropic samples such as SWNTs require additional measurements by other means as will be described in the following section.

The relative uncertainties reported are one standard deviation, based on the goodness of the fit or from multiple runs. Total combined uncertainties from all external sources are not reported, as comparisons are made with data obtained under the same conditions. In cases where the limits are smaller than the plotted symbols, the limits are left out for clarity.

Certain equipment, instruments, or materials are identified in this paper in order to adequately specify the experimental

1844 *J. Phys. Chem. C, Vol. 112, No. 6, 2008*

Bauer et al.

details. Such identification does not imply recommendation by the National Institute of Standards and Technology nor does it imply the materials are necessarily the best available for the purpose.

Light Scattering Theory

Scattering theory for isotropic structures is well-established and models are available for fitting MALS data to obtain size and shape information for a variety of objects. A dilute solution of objects scatters light at an angle Θ as

$$I(q) = K^* M c P(q) \tag{1}$$

where $I(q)$ is the light scattered in absolute intensity units, M is the molar mass of the scatterer, and c is the concentration. K^* and q are defined as

$$K^* = \frac{4\pi^2 n_0^2}{N_A \lambda_0^4} \left(\frac{dn}{dc}\right)^2 \tag{2}$$

$$q = \frac{4\pi \sin(\Theta/2)}{\lambda_0/n_0} \tag{3}$$

where n_0 is the refractive index of the liquid, λ_0 is the wavelength of the incident light, and N_A is Avogadro's number. The refractive index increment, dn/dc, is the rate of change of the solution's refractive index with the addition of mass concentration c of scatterer. $P(q)$ is the form factor of the object and has been calculated for a variety of structures.

While the scattering from an isotropic distribution of non-interacting thin rigid rods is well-established,[38] when the rods are both absorbing and birefringent, some modification is required. For the geometry of interest, we consider N optically anisotropic absorbing rods of individual volume v in a total volume V, for which the scattering intensity is $I(\mathbf{q}) \propto V^{-1}|\hat{\mathbf{z}}\cdot\delta \overset{\leftrightarrow}{\epsilon}_{\mathbf{q}}|^2$, where $\hat{\mathbf{z}}$ defines the polarization of the incident light and

$$\delta \overset{\leftrightarrow}{\epsilon}_{\mathbf{q}} = \sum_{l=1}^{N} (A\hat{\mathbf{n}}_l\hat{\mathbf{n}}_l + B\mathbf{1})\, e^{-i\mathbf{q}\cdot\mathbf{r}_l} f_l(\mathbf{q}) \tag{4}$$

is the scattering amplitude tensor.[39] In eq 4, $\hat{\mathbf{n}}_l$ is the unit director of the lth rod, $A = \epsilon_\parallel - \epsilon_\perp$, $B = \epsilon_\perp - \epsilon_0$, and $f_l(\mathbf{q}) = \int_{v_l} e^{-i\mathbf{q}\cdot\mathbf{r}} d\mathbf{r}$. The constants $\epsilon_\parallel$ and $\epsilon_\perp$ are the complex dielectric response function intrinsic to the rod, while ϵ_0 is the dielectric constant of the suspending medium. The subscripts $\parallel$ and $\perp$ denote the polarization along and normal to the rod axis. In the absence of rod−rod interactions, this becomes

$$I(\mathbf{q}) \propto \sum_l (|A|^2 + 2\mathrm{Re}(AB^*))(\hat{\mathbf{n}}_l\cdot\hat{\mathbf{z}})^2 |f_l(\mathbf{q})|^2 +$$

$$\sum_l |B|^2 |f_l(\mathbf{q})|^2 \tag{5}$$

which for $\epsilon_\parallel = \epsilon_\perp$ ($A = 0$) reduces to the well-known result for nonbirefringent rods;

$$I(\mathbf{q}) \propto \sum_l |f_l(\mathbf{q})|^2 \propto v\phi \left\{ \frac{2S_i(qL)}{qL} - \frac{2 - 2\cos(qL)}{(qL)^2} \right\} \tag{6}$$

where L is the rod length, ϕ is the volume fraction, q is the scattered wave vector, and $S_i(x) = \int_0^x du \sin u/u$ is the sine integral function. Physically, the effect of the optical anisotropy is to introduce an additional term in the scattering amplitude

weighted by the orientation of each rod with respect to the direction of incident polarization. Measurements of the effective intrinsic optical anisotropy for CoMoCAT SWNTs of mean length approximately 300 nm have recently been performed over a broad spectral range.[37] At $\lambda = 690$ nm, these measurements give $\epsilon_\parallel = \epsilon_\parallel' + i\epsilon_\parallel'' \approx 3.99 + 2.04i$ and $\epsilon_\perp = \epsilon_\perp' + i\epsilon_\perp'' \approx 1.52 + 0.65i$, with $\epsilon_0 = (1.33)^2 = 1.77$ for water. The constants $A = 2.47 + 1.39i$ and $B = -0.25 + 0.65i$ thus give the relative weighting of the two terms in eq 5;

$$I(\mathbf{q}) \propto (0.48) \sum_l |f_l(\mathbf{q})|^2 + (8.57) \sum_l \cos^2 \theta_l |f_l(\mathbf{q})|^2 \equiv I_1 + I_2 \tag{7}$$

where θ_l is the angle the lth SWNT makes with the z axis. The relative values of the dielectric response for the solvent and the solute are within the range of applicability of eq 4. Within a common constant factor, the two terms in eq 7 reduce to

$$I_1 = (0.48)\left\{ \frac{2S_i(qL)}{qL} - \frac{2 - 2\cos(qL)}{(qL)^2} \right\} \tag{8}$$

and

$$I_2 = \frac{8.57}{4\pi} \int d\Omega \cos^2\theta \left\{ \frac{2}{(Lq_z \cos\theta + Lq_\perp \cos\phi \sin\theta)} \right. $$
$$\left. \sin\left(\frac{Lq_z \cos\theta + Lq_\perp \cos\phi \sin\theta}{2}\right) \right\}^2 \tag{9}$$

The projection of interest is $q_z = 0$, so the second, anisotropic term becomes

$$I_2 = \frac{8.57}{4\pi} \int_0^{2\pi} d\phi \int_0^\pi d\theta$$
$$\sin\theta \cos^2\theta \left\{ \frac{4}{(Lq \cos\phi \sin\theta)^2} \sin^2\left(\frac{Lq \cos\phi \sin\theta}{2}\right) \right\} \tag{10}$$

$$I_2 = 8.57\left\{ \frac{S_i(qL)}{qL} - \frac{2 - \cos(qL)}{(qL)^2} + \frac{\sin(qL)}{(qL)^3} \right\} \tag{11}$$

Both I_1 and I_2 can be evaluated numerically. In absolute units, the total scattering intensity follows by analogy with the classical scattering expression first derived by Zimm;[38]

$$I = \frac{\pi^2 n_0^4 M\phi}{\rho\lambda_0^4 N_A} (I_1 + I_2) \tag{12}$$

where $\phi = Nv/V = c/\rho$ is the volume fraction of SWNT and $\rho = m/v = 1.0$ g/cm^3 is the SWNT density. Equations 1−3 and 12 can be combined to calculate "equivalent" values of dn/dc and $P(q)$ for the anisotropic SWNT rods

$$\text{equivalent } \frac{dn}{dc} = (I_1(q \to 0) + I_2(q \to 0))^{1/2} \frac{n_0}{2\rho} = 1.22 \text{ mL/g} \tag{13}$$

$$P(q) = \frac{I_1 + I_2}{I_1(q \to 0) + I_2(q \to 0)} \tag{14}$$

The scattering from anisotropic rods is considerably different from isotropic rods due to these changes in the equivalent dn/dc and $P(q)$ that cause major differences in calculated molar mass and rod length. For example, the calculated molar mass is proportional to the inverse square of the dn/dc used, so that
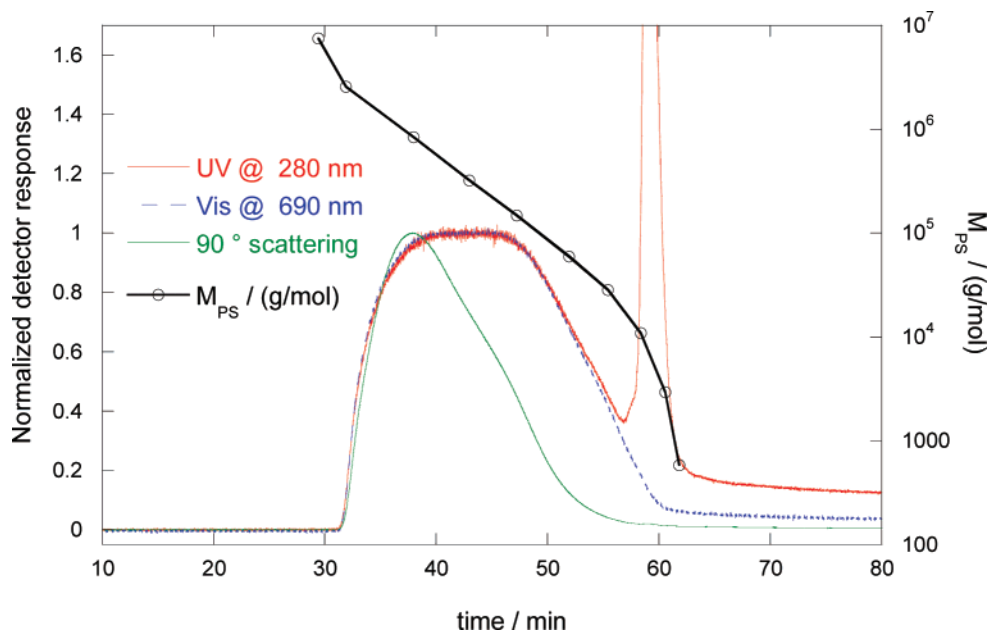
Chromatographic Fractionation

J. Phys. Chem. C, Vol. 112, No. 6, 2008 **1845**

Figure 1. Typical chromatogram of SWNT/DNA dispersion. Vis absorption at 690 nm detects only SWNT while UV absorption at 280 nm detects both SWNT/DNA and unattached DNA. MALS at 90° angle has stronger signal at early times, indicating larger SWNTs are eluting at early times. Calibration of PS in THF shows the exclusion limits of the column that span the range of 500 nm SWNT/DNA to unattached DNA. After this limit for the SEC mechanism, a small amount of material continues to elute in a HPLC mechanism.

the molar mass calculated from an isotropic model is $(1.22/0.373)^2 = 10.7$ times larger than that from an anisotropic model.

Results

Figure 1 is a plot of SEC of a typical SWNT/DNA dispersion with UV−vis photodiode array detector along with a MALS detector. The absorption at 690 nm is due to the SWNT content alone, since the DNA is transparent at this wavelength. The absorption at 280 nm is due to both the SWNT and the DNA. The normalized absorption at these two wavelengths overlaps at elution times below 57 min, but the 280 nm absorption shows a sharp peak at about 59 min that is due to unattached DNA. The normalized 90° detector signal is a measure of light scattering intensity at 90° from the incident beam. The shape of the 90° detector signal is skewed to the shorter times producing a larger 90° detector signal/concentration ratio at early times indicating higher molar mass solute eluting at earlier times.

SEC shows an early time limit, below which no injected material elutes. The material is large enough to be excluded from entering any of the pores and is carried along with the solvent between the particles. It can be seen at about 31 min where a sharp rise in signal from the detectors begins. There is also a late time limit that occurs when the minimum pore size is larger than all remaining eluents, and all material smaller than this pore size elutes at the same time. The SEC mechanism alone cannot cause injected material to elute after this limit.

The maximum SEC time limit for the data in Figure 1 is approximately 63 min. However, inspection of the UV, vis, and MALS detector response shows a small but nonzero response after this time. This response is evidence that material from the initial injection is still eluting. This means that the SEC mechanism alone cannot be the only factor in the separation. It is likely that a HPLC mechanism is causing eluents to emerge after the SEC exclusion maximum time limit. The signal from the detectors drops with time and is negligible by the time the next injection is made, since MALS fits can be made at long times, but only baseline scattering exists by the start of the next run. Zheng et al.[25] also show this effect, as can be seen in Figure

1 (in their paper). The chromatogram at times after the elution of their unattached DNA peak does not return to the baseline that was present at early times. It is likely that the SWNT/DNA was also eluting by a HPLC mechanism at this point in their separation.

Before the aqueous runs, the SEC columns were flushed with tetrahydrofuran (THF) and injections of mixed polystyrene (PS) in THF were made. The column sets used in this study were capable of separations in both aqueous and organic solvents, and the column separation limits can be compared. The elution time of 10 polystyrenes (PS) with molar masses from 580 to 7 500 000 g/mol in THF is also plotted in Figure 1. The PS elution times drop linearly with their log (molar mass) over the middle of the SWNT/DNA peak but turn up or down sharply at the two exclusion limits. This is typical of organic SEC in good solvents done with a mixed bed column, and no PS elution is seen outside of the two expected exclusion limits.

The MALS was recorded at seven angles throughout the elution, and fits were made of the intensity and angular dependence. Figure 2 is a plot of the scattered intensity of a typical SWNT/DNA dispersion taken at 35.1 min. The scattered intensity is normalized to sample concentration and instrument constants. The data are in absolute intensity units as a function of the scattering angle converted to scattering vector, q, by the use of eq 3. A monodisperse isotropic rigid rod was fit with eqs 1 and 2 using a standard isotropic rod $P(q)$, and a monodisperse anisotropic rigid rod was fit with eq 12. Each of the monodisperse objects produces a poor fit of the data. The anisotropic rod fit is slightly better than the isotropic rod fit, but neither of these monodisperse models fit the scattering from the solute over the entire angular range. The available range of our MALS is between the Guiner region and the power law region, $0.4 < q\,Rg < 2.8$. Therefore, the calculation of Rg from a Guinier analysis will not fulfill the requirement $q\,Rg \ll 1$ at low q, and the power law region $q\,Rg \gg 1$ will not give the limiting rod exponent of -1. This is why the more complicated analysis of using the full expression for $P(q)$ is necessary. The fits to the data are detailed in Supporting Information.
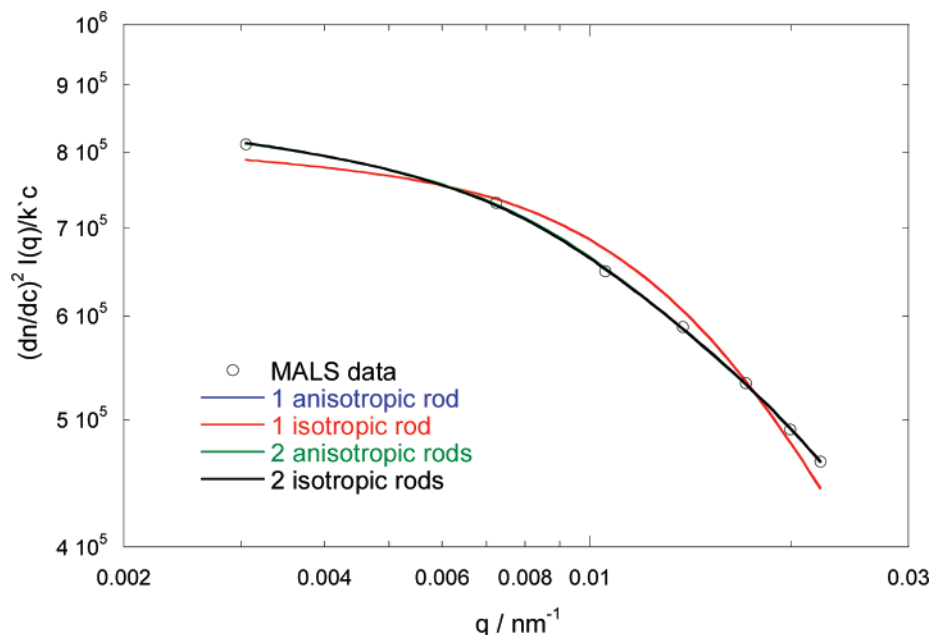
Figure 2. Fits of MALS at 35.1 min elution time to rod functions. Models for monodisperse anisotropic rods and isotropic rods give poor fits. Models for bimodal anisotropic rods or isotropic rods have greatly improved fits, but it is not possible to identify the structure of polydisperse samples by these fitting methods alone.

The discrepancies between the data and the fit in Figure 2 may be due to polydispersity. Equations 15 and 16 are the $P(q)$ from a binary isotropic rod (eq 6) mixture and a binary anisotropic rod (eq 12) mixture, respectively. w_i is the mass fraction of component i.

$$P_{IR}(q) = w_1 M_1 P_{\text{isotropic rod1}}(q) + w_2 M_2 P_{\text{isotropic rod2}}(q) \quad (15)$$

$$P_{AR}(q) = w_1 M_1 P_{\text{anisotropic rod1}}(q) + w_2 M_2 P_{\text{anisotropic rod2}}(q) \quad (16)$$

The polydisperse functions significantly improve the fit to the data as seen in Figure 2 suggesting that polydispersity of some form is accounting for the shape of the experimental data. However, the fits of either a binary rod mixture or more complex distributions of rods, coils or spheres can all fit the data adequately with eq 12 providing the best fit. Therefore, the shape of the scattering alone is not sufficient to determine the structure. Distinguishing the structure is possible, however, by using the ability of SEC to separate by size. As an example, eq 16 was used to fit the MALS over the whole range of the chromatogram using the fitting parameters $w_1 M_1$, $w_2 M_2$, L_1, and L_2. This fitting method assumes that the solute is made up of mixtures of two monodisperse rods, which is quite unlikely. However, in the absence of information on the true distribution, it is an effective "equivalent" distribution that can be used to extract important information from the experimental data. Various distributions were fit to the MALS data, all producing similar values for the molar mass and length averages, and the bimodal distribution will be used as a representative example. The polydispersity at a single time increment can be calculated from the shape of the scattering curve but is less important than the total polydispersity of the whole SWNT sample. The polydispersity of the whole sample can be calculated by adding the contributions of each increment.

Eight identical SEC runs were made using the same initial SWNT/DNA dispersion. Fits of the raw data were made and statistical analysis of the results were done to produce averages and uncertainties of one standard deviation. Figure 3 is a plot of the calculated mass average M and L from the fits of eq 16. The parameters of interest need to be calculated from the fitting

parameters. M_W is a mass-average molar mass of the M fit parameters as calculated by eq 17.

$$M_W = w_1 M_1 + w_2 M_2 \quad (17)$$

An equivalent mass average rod length, L_W, needs to be calculated, but the weight fractions need to be estimated first. If the assumption of a rod structure of the solute is valid, then the ratio of the molar mass to the rod length M_i/L_i will be a constant and the mass fractions can be calculated from the fitting parameters. Also with this assumption, number fractions n_i and number average molar mass, M_N can be calculated.

$$L_W = w_1 L_1 + w_2 L_2 \quad (18)$$

$$w_1 = \frac{w_1 M_1/L_1}{w_1 M_1/L_1 + w_2 M_2/L_2} = 1 - w_2 \quad (19)$$

$$M_N = n_1 M_1 + n_2 M_2 \quad (20)$$

$$n_1 = \frac{w_1/M_1}{w_1/M_1 + w_2/M_2} = 1 - n_2 \quad (21)$$

Figure 3 shows a uniform decrease in both L and M at early times. The fact that they are parallel in this region suggests a proportionality of $L \propto M^{1.0}$, which is characteristic of a rigid rod. The M value reaches a minimum at about the time that the unattached DNA peak arrives. Beyond this time, the M increases to a relatively constant value, but it is representative of only a small portion of the original injected SWNT/DNA mass compared with the main peak as is shown by the relative concentration in Figure 3. It is likely that this is due to small amounts of SWNT being slowly desorbed from the columns through a HPLC mechanism. Similarly, L reaches a minimum at a slightly earlier time than the M and increases to a constant value past the SEC exclusion limit.

Figure 4 plots the L versus M data with a line showing a linear relationship. The line shown has a power law of 1.0, which would be the case for rigid rods. The data points before
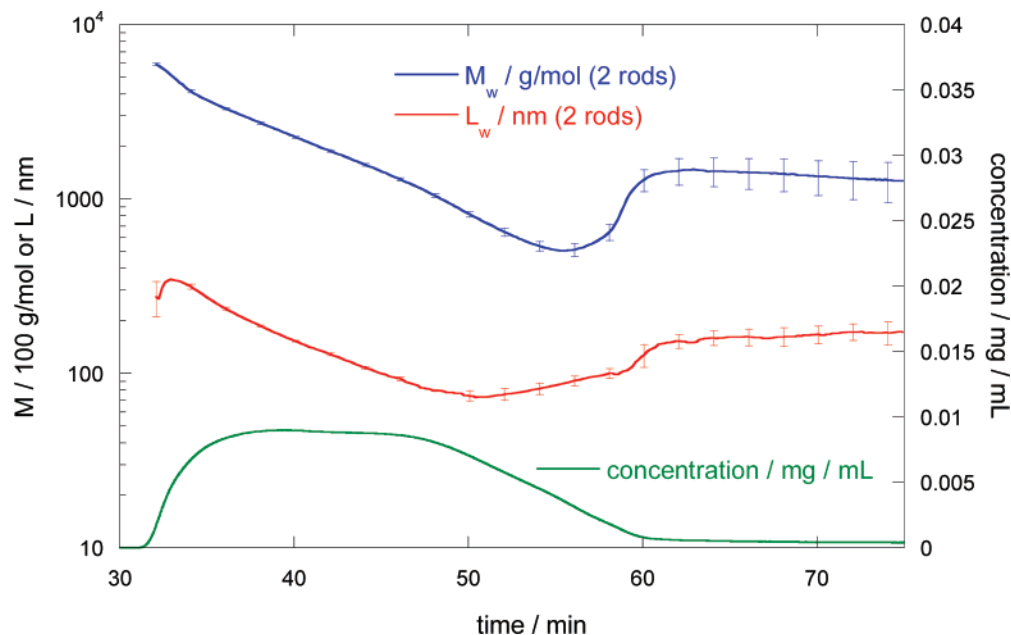
Chromatographic Fractionation

J. Phys. Chem. C, Vol. 112, No. 6, 2008 **1847**

Figure 3. Fits of L_W and M_W from bimodal rods are shown. An exponential decrease in each is present up to 50 min. At longer times, both L and M increase in size even beyond the normal SEC limits, suggesting an adsorption HPLC-like mechanism.
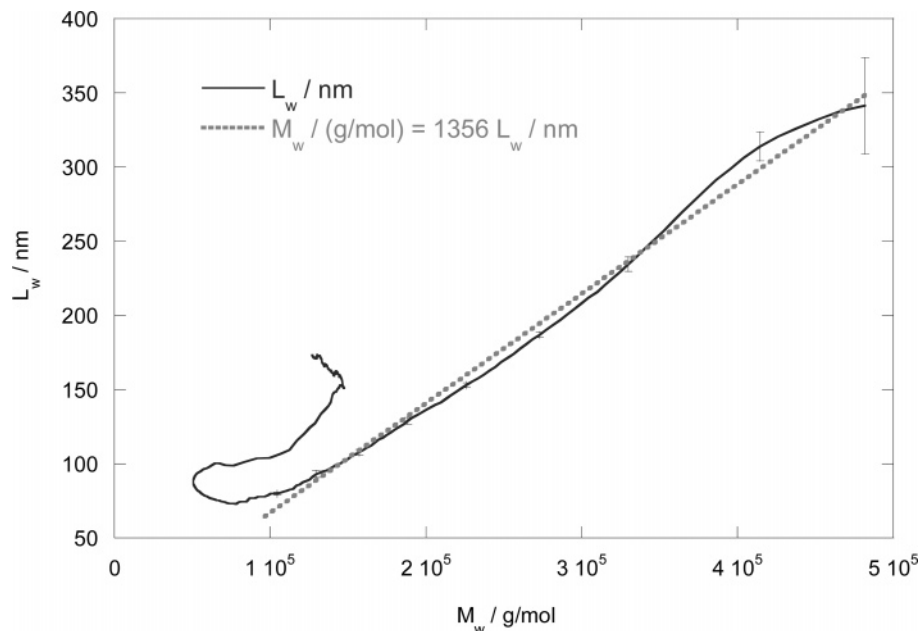

Figure 4. Plot of L_W vs M_W has a 1.0 power law over a considerable range. This is characteristic of an extended rod. Most of the mass of the SWNT dispersion resides in this power law range. The line shown is for a M/L ratio of 1356 AMU/nm.

48 min elution time are consistent with rod like SWNT/DNA dispersions. After this time, the points form a relatively tight cluster at the low end of the size range. This is consistent with a separation mechanism that is predominately SEC earlier than 48 min and a separation mechanism at later times that becomes increasingly influenced by the HPLC mechanism. The slope at early times is insensitive to the model of the $P(q)$ fitting but is only meaningful for a rigid rod. This validated the assumption of a rigid rod $P(q)$ fitting function and the calculation of w_i from eq 19 that also assumes that L is proportional to M.

The ratio of M to L from Figure 4 can be compared to theoretical values that can be calculated for any particular chirality. The diameter of a SWNT with (n,m) chirality can be easily calculated.[40] CoMoCAT SWNTs are predominately (6,5) chirality that have diameters of 0.75 nm and a M/L ratio of 1612 AMU/nm. The line in Figure 4 has a slope of 1365 AMU/

nm that is within 20% of the theoretical value. If the isotropic rod model is used and dn/dc data are used as described previously, the M/L ratio is more than 10 times greater than the value calculated from the anisotropic model. This is further confirmation of the need for an anisotropic model for SWNT data analysis.

The polydispersity index (PDI) can be calculated as a ratio of M_W/M_N from eq 17 and eq 20. Figure 5 shows that the initial long SWNTs have a broad distribution, consistent with the exclusion limit that has only a weak ability to separate by size as in shown by the PS curve in Figure 1. The PDI drops rapidly as the size scale reaches the linear region of the separation range, reaching a minimum of about 1.1 before increasing. This increase is consistent with a mixed SEC and HPLC separation mechanism. At the longest times the PDI levels off, but the low concentrations cause a large uncertainty.
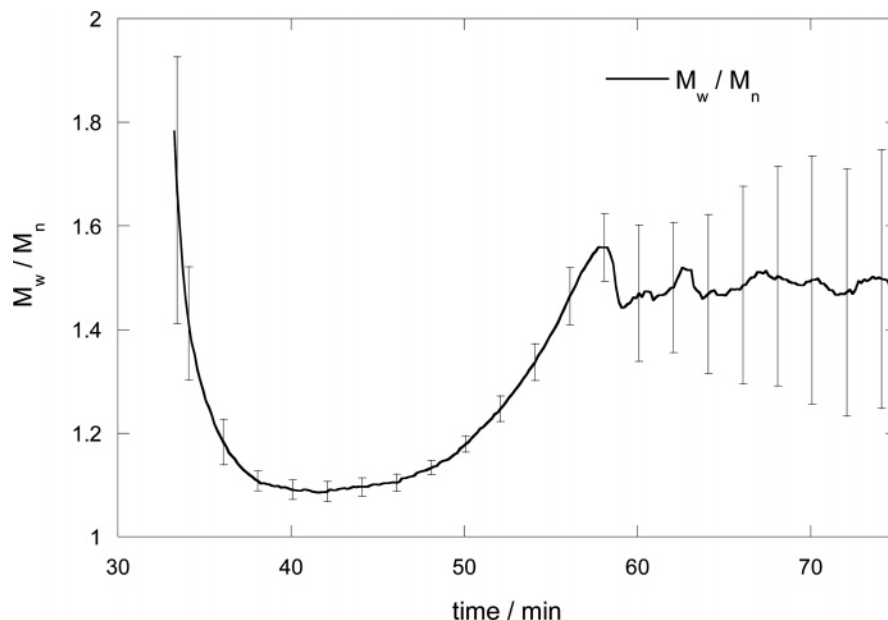
Figure 5. Polydispersity, M_W/M_N, of SWNTs as a function of elution time from $P(q)$ fits. There is high polydispersity at the early exclusion limit that drops sharply. The polydispersity increases as the time approaches and exceeds the late exclusion limit.

The PDI that is calculated from the shape of the MALS data alone provides insight into the separation mechanism, but a PDI representative of the whole SWNT sample is useful in comparing batch-to-batch uniformity. The PDI of the whole sample can be calculated from the contributions of each increment summed throughout the entire chromatogram. The molar mass values from Figure 3 are averaged throughout the entire distribution weighted by the relative mass from the concentration detector. Equations 17–21 are used to calculate M_{Ni} and M_{Wi} for each 10 s increment of MALS, and molar mass averages and polydispersity from the entire distribution are calculated with eqs 22 and 23.

$$M_N = \frac{\sum_i C_i}{\sum_i C_i/M_{Ni}} \tag{22}$$

$$M_W = \frac{\sum_i M_{Wi}C_i}{\sum_i C_i} \tag{23}$$

C_i is the SWNT concentration calculated from the absorption at 690 nm. The average of the 8 SWNT/DNA samples is $M_W = (1.84 \pm 0.08) \times 10^5$ g/mol, $M_N = (1.02 \pm 0.05) \times 10^5$ g/mol, and $M_W/M_N = (1.81 \pm 0.03)$. The total polydispersity of all of the increments combined is significantly higher than those calculated for the individual increments.

To gain additional information on the nature of the separation, several repeat runs were made and samples were collected at early and late stages in the SEC separation. Appropriate samples were combined and concentrated for re-injection. Figure 6 shows the UV−vis absorption at (280 and 690) nm of the starting, unfractionated SWNT/DNA and the two fractions. The bars at the top show the collection times for the early and late fractions. Figure 6a is a typical separation showing a broad peak with a narrow peak at 280 nm due to unattached DNA. Figure 6c has a prominent peak at about the same time range that the sample

collection took place. There is a feature in the absorption at 280 nm that is likely due to DNA and DNA dimer. This sample was re-injected approximately 3 months after the fraction collection. It seems that in this period a small amount of DNA has unwrapped from the SWNT/DNA. A slow equilibrium may be present between DNA wrapped around the SWNT and the DNA in solution. The fractionation has removed the free DNA, so that slow unwrapping is a response to the new equilibrium. Also of note in Figure 6C is the weak "tail" of the main peak at longer times. Both absorption and MALS detectors see this material, and the size is close to that of the main peak. It is likely that the collected fractions, when refractionated, again have a portion of their mass delayed by a HPLC mechanism.

The late fraction also eluted near the collection time of the original fractions but now has a weak "tail" at shorter times. This is consistent with the original fraction collecting both short SWNTs through a SEC mechanism and a small amount of long SWNTs through a HPLC mechanism. Upon reinjection, most of the long SWNTs elute by the SEC mechanism, causing the tail. MALS from this early region of the injection shows the tail to be of long SWNTs. The results of these re-injections suggest that the mixture of SEC and HPLC separation mechanisms is dominated by the SEC mechanism at early times, that results in only a slight broadening of the sample distributions in the collected fractions due to the HPLC mechanism.

A number of laboratories have used sonication for extended periods to generate a number of samples with different average lengths through fracture of the SWNTs.[3,4] Typically, sonication is continued over many hours or days and samples are removed throughout this time period. While there is clearly a change in average length, the breadth of the distribution is generally not known. To quantify this effect and compare its processing capabilities to the fractionation achieved by SEC, a single batch of material was sonicated for 3 different lengths of time (2, 14, and 27 h), and samples were injected into the SEC. Figure 7 shows the adsorption at 690 nm from the three sonicated samples along with the two re-injected ones from Figure 6. Extended sonication clearly lowers the average SWNT length in the solution, but the breadth of the distributions in the sonicated samples is considerably greater than for the SEC fractions. Even
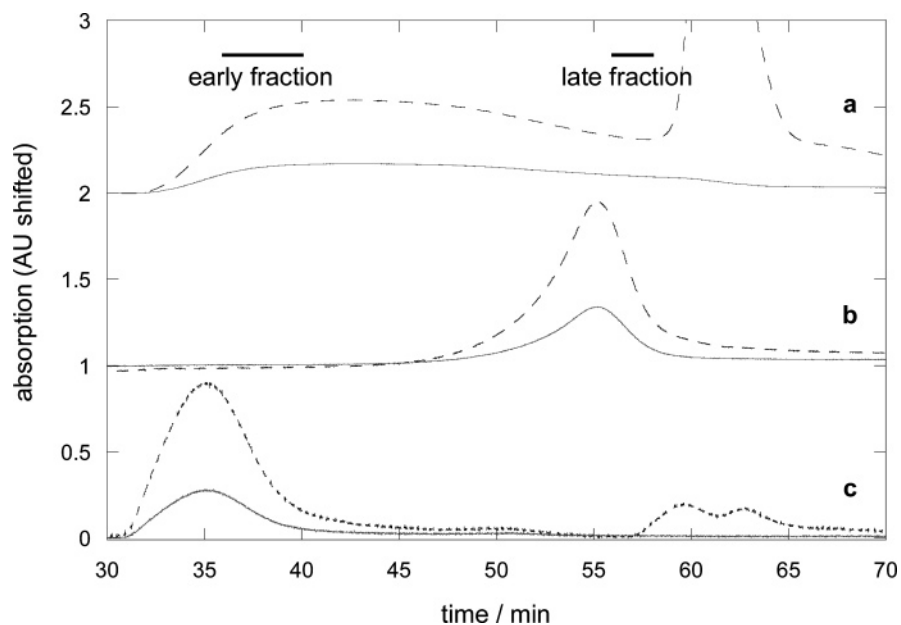
Chromatographic Fractionation

J. Phys. Chem. C, Vol. 112, No. 6, 2008 **1849**

Figure 6. SEC of initial dispersions (a) and re-injected fractions from late (b) and early (c) times. The dotted lines are absorption at 280 nm, and the solid lines are absorption at 690 nm. A majority of the fractions elute at a time consistent with the original collection window, but broadened "tails" occur to the early time side of the late fraction and the late time side of the early fraction. The early fractions have 280 nm absorption peaks at 60 min, indicating that some of the DNA has desorbed from the SWNTs.
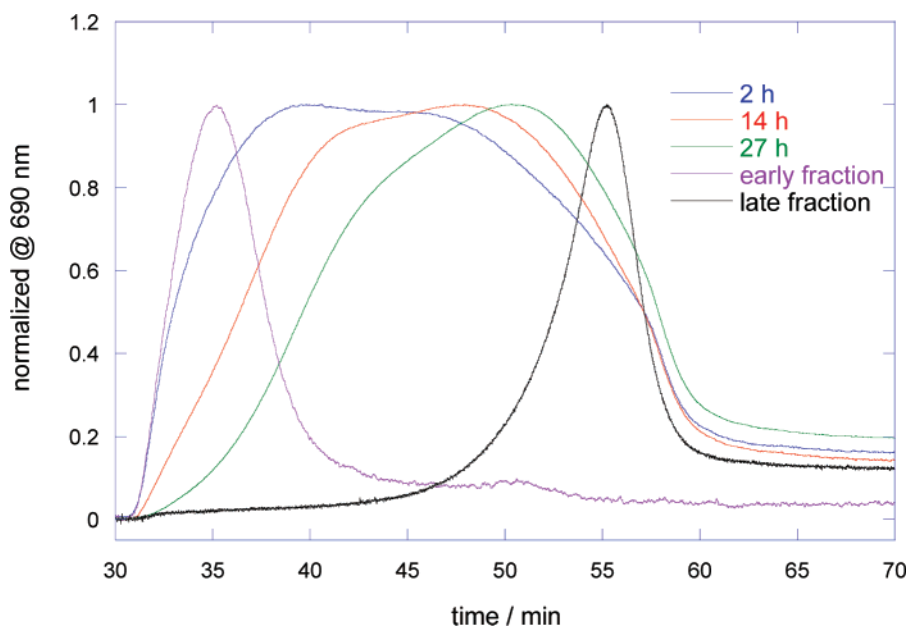

Figure 7. SEC chromatograms of SWNT/DNA dispersions sonicated for (2, 14, and 27) hours and the early and late fractions from Figure 6b,c. Despite the minor "tailing" of the SEC fractions, the width of the distribution is considerably narrower than the samples fractured via sonication to produce shorter SWNTs.

with the complication of mixed separation mechanisms, SEC fractions produce samples that are considerably narrower, and over a much wider length range, than those possible by fracture methods.

Summary

SEC is an important method for size fractionation of SWNTs. Dispersions with DNA are efficiently separated into narrow fractions. The runs described in this manuscript were typically 0.5 mL injections of 0.4 mg/mL SWNT dispersions. Up to thirty fractions were then collected yielding an approximate average of 0.01 mg per sample. Using ultrafiltration, repeat runs of the SEC process can be performed, and fractions can easily be combined and concentrated; in the process of this work, 18 repeats were performed, and the quantities produced were sufficient to investigate both biological uptake effects of SWNT length[34] and the length dependence of the SWNT optical properties.[35] Additionally, the columns used in this study are also available in larger diameters, allowing for scale-up to larger quantities. Thus, narrow fractions in the milligram range are possible by use of SEC in a practical period of time.

On-line MALS is a valuable addition to SEC for determination of molar mass and rod length of the dispersed SWNTs. The scattering is strong and reproducible and can detect subtle effects in the size distributions of the fractions generated. The separations reported herein were conducted on SWNTs dispersed in salt solution (0.2 mol/L NaCl, 0.04 mol/L Tris, HCl to pH = 7.0) in the presence of 1 mg/mL 30-mer 5′-GT(GT)$_{13}$GT-3′

Bauer et al.

single stranded DNA. The results demonstrate that the predominate separation mechanism is size exclusion with the longest and highest molar mass SWNTs eluting first and then continuously decreasing in size range from approximately 500 to 50 nm. Near the long time limit of the SEC, a second separation mechanism was shown to become important because of solute adsorption on the column material as in a HPLC mechanism separation. Small amounts of longer SWNT slowly come off of the column even after the long time exclusion limit of the column. While this adds slightly to the polydispersity of the fractions collected, reruns of the SEC fractions are considerably narrower than "fractions" produced by sonication fracturing of long SWNTs.

Furthermore, these results show that, over the initial separation range that is dominated by a SEC mechanism, the rod length and molar mass change with a power law of 1.0, characteristic of rigid rods and suggesting an extended SWNT conformation in solution. The ratio M/L is also consistent with rodlike behavior of the SWNTs.

Supporting Information Available: Details on the measurement of the refractive index increment. This information is available free of charge via the Internet at http://pubs.acs.org.

References and Notes

(1) Baughman, R. H.; Zakhidov, A. A.; de Heer, W. A. Carbon nanotubes - the route toward applications. *Science* **2002**, *297* (5582), 787–792.

(2) Haddon, R. C.; Sippel, J.; Rinzler, A. G.; Papadimitrakopoulos, F. Purification and separation of carbon nanotubes. *MRS Bull.* **2004**, *29* (4), 252–259.

(3) Krupke, R.; Hennrich, F. Separation techniques for carbon nanotubes. *Adv. Eng. Mater.* **2005**, *7* (3), 111–116.

(4) Arnold, M. S.; Stupp, S. I.; Hersam, M. C. Enrichment of single-walled carbon nanotubes by diameter in density gradients. *Nano Lett.* **2005**, *5* (4), 713–718.

(5) Arnold, M. S.; Green, A. A.; Hulvat, J. F.; Stupp, S. I.; Hersam, M. C. Sorting carbon nanotubes by electronic structure using density differentiation. *Nature Nanotechnol.* **2006**, *1* (1), 60–65.

(6) Doorn, S. K.; Fields, R. E.; Hu, H.; Hamon, M. A.; Haddon, R. C.; Selegue, J. P.; Majidi, V. High resolution capillary electrophoresis of carbon nanotubes. *J. Am. Chem. Soc.* **2002**, *124* (12), 3169–3174.

(7) Doorn, S. K.; Strano, M. S.; O'Connell, M. J.; Haroz, E. H.; Rialon, K. L.; Hauge, R. H.; Smalley, R. E. Capillary electrophoresis separations of bundled and individual carbon nanotubes. *J. Phys. Chem. B* **2003**, *107* (25), 6063–6069.

(8) Suarez, B.; Simonet, B. M.; Cardenas, S.; Valcarcel, M. Separation of carbon nanotubes in aqueous medium by capillary electrophoresis. *J. Chromatogr., A* **2006**, *1128* (1–2), 282–289.

(9) Zheng, M.; Jagota, A.; Strano, M. S.; Santos, A. P.; Barone, P.; Chou, S. G.; Diner, B. A.; Dresselhaus, M. S.; Mclean, R. S.; Onoa, G. B.; Samsonidze, G. G.; Semke, E. D.; Usrey, M.; Walls, D. J. Structure-based carbon nanotube sorting by sequence-dependent DNA assembly. *Science* **2003**, *302* (5650), 1545–1548.

(10) Zheng, M.; Jagota, A.; Semke, E. D.; Diner, B. A.; Mclean, R. S.; Lustig, S. R.; Richardson, R. E.; Tassi, N. G. DNA-assisted dispersion and separation of carbon nanotubes. *Nat. Mater.* **2003**, *2* (5), 338–342.

(11) Chen, B. L.; Selegue, J. P. Separation and characterization of single-walled and multiwalled carbon nanotubes by using flow field-flow fractionation. *Anal. Chem.* **2002**, *74* (18), 4774–4780.

(12) Liu, J.; Rinzler, A. G.; Dai, H. J.; Hafner, J. H.; Bradley, R. K.; Boul, P. J.; Lu, A.; Iverson, T.; Shelimov, K.; Huffman, C. B.; Rodriguez-Macias, F.; Shon, Y. S.; Lee, T. R.; Colbert, D. T.; Smalley, R. E. Fullerene pipes. *Science* **1998**, *280* (5367), 1253–1256.

(13) Moon, M. H.; Kang, D. J.; Jung, J. H.; Kim, J. M. Separation of carbon nanotubes by frit inlet asymmetrical flow field-flow fractionation. *J. Sep. Sci.* **2004**, *27* (9), 710–717.

(14) Peng, H. Q.; Alvarez, N. T.; Kittrell, C.; Hauge, R. H.; Schmidt, H. K. Dielectrophoresis field flow fractionation of single-walled carbon nanotubes. *J. Am. Chem. Soc.* **2006**, *128* (26), 8396–8397.

(15) Lee, J.; Jeong, T.; Heo, J.; Park, S. H.; Lee, D.; Park, J. B.; Han, H.; Kwon, Y.; Kovalev, I.; Yoon, S. M.; Choi, J. Y.; Jin, Y. W.; Kim, J. M.; An, K. H.; Lee, Y. H.; Yu, S. Short carbon nanotubes produced by cryogenic crushing. *Carbon* **2006**, *44* (14), 2984–2989.

(16) Pierard, N.; Fonseca, A.; Colomer, J. F.; Bossuot, C.; Benoit, J. M.; Van Tendeloo, G.; Pirard, J. P.; Nagy, J. B. Ball milling effect on the structure of single-wall carbon nanotubes. *Carbon* **2004**, *42* (8–9), 1691–1697.

(17) Zhang, J.; Zou, H. L.; Qing, Q.; Yang, Y. L.; Li, Q. W.; Liu, Z. F.; Guo, X. Y.; Du, Z. L. Effect of chemical oxidation on the structure of single-walled carbon nanotubes. *J. Phys. Chem. B* **2003**, *107* (16), 3712–3718.

(18) Ziegler, K. J.; Gu, Z. N.; Shaver, J.; Chen, Z. Y.; Flor, E. L.; Schmidt, D. J.; Chan, C.; Hauge, R. H.; Smalley, R. E. Cutting single-walled carbon nanotubes. *Nanotechnology* **2005**, *16* (7), S539–S544.

(19) Ziegler, K. J.; Gu, Z. N.; Peng, H. Q.; Flor, E. L.; Hauge, R. H.; Smalley, R. E. Controlled oxidative cutting of single-walled carbon nanotubes. *J. Am. Chem. Soc.* **2005**, *127* (5), 1541–1547.

(20) Arnold, K.; Hennrich, F.; Krupke, R.; Lebedkin, S.; Kappes, M. M. Length separation studies of single walled carbon nanotube dispersions. *Phys. Status Solidi B* **2006**, *243* (13), 3073–3076.

(21) Chattopadhyay, D.; Lastella, S.; Kim, S.; Papadimitrakopoulos, F. Length separation of Zwitterion-functionalized single wall carbon nanotubes by GPC. *J. Am. Chem. Soc.* **2002**, *124* (5), 728–729.

(22) Duesberg, G. S.; Muster, J.; Krstic, V.; Burghard, M.; Roth, S. Chromatographic size separation of single-wall carbon nanotubes. *Appl. Phys. A* **1998**, *67* (1), 117–119.

(23) Duesberg, G. S.; Burghard, M.; Muster, J.; Philipp, G.; Roth, S. Separation of carbon nanotubes by size exclusion chromatography. *Chem. Commun.* **1998**, (3), 435–436.

(24) Farkas, E.; Anderson, M. E.; Chen, Z. H.; Rinzler, A. G. Length sorting cut single wall carbon nanotubes by high performance liquid chromatography. *Chem. Phys. Lett.* **2002**, *363* (1–2), 111–116.

(25) Huang, X. Y.; Mclean, R. S.; Zheng, M. High-resolution length sorting and purification of DNA-wrapped carbon nanotubes by size-exclusion chromatography. *Anal. Chem.* **2005**, *77* (19), 6225–6228.

(26) Yang, Y. L.; Xie, L. M.; Chen, Z.; Liu, M. H.; Zhu, T.; Liu, Z. F. Purification and length separation of single-walled carbon nanotubes using chromatographic method. *Synth. Met.* **2005**, *155* (3), 455–460.

(27) Schimpt, M. E., Caldwell, K., Giddings, J. C., Eds. *Field Flow Fractionation Handbook;* Wiley-Interscience: New York, 2000.

(28) Mori, S.; Barth, H. G. *Size Exclusion Chromatography;* Springer: Berlin, 1999.

(29) Byrd, H. C. M.; Bencherif, S. A.; Bauer, B. J.; Beers, K. L.; Brun, Y.; Lin-Gibson, S.; Sari, N. Examination of the covalent cationization method using narrow polydisperse polystyrene. *Macromolecules* **2005**, *38* (5), 1564–1572.

(30) Duesberg, G. S.; Blau, W.; Byrne, H. J.; Muster, J.; Burghard, M.; Roth, S. Chromatography of carbon nanotubes. *Synth. Met.* **1999**, *103* (1–3), 2484–2485.

(31) Schaefer, D.; Brown, J. M.; Anderson, D. P.; Zhao, J.; Chokalingam, K.; Tomlin, D.; Ilavsky, J. Structure and dispersion of carbon nanotubes. *J. Appl. Crystallogr.* **2003**, *36*, 553–557.

(32) Schaefer, D. W.; Zhao, J.; Brown, J. M.; Anderson, D. P.; Tomlin, D. W. Morphology of dispersed carbon single-walled nanotubes. *Chem. Phys. Lett.* **2003**, *375* (3–4), 369–375.

(33) Cotts, P. M. Light scattering of DNA-carbon nanotubes in aqueous suspension. *Abs. Am. Chem. Soc.* **2005**, *230*, U3511–U3513.

(34) Becker, M. L.; Fagan, J. A.; Gallant, N. D.; Bauer, B. J.; Bajpai, V.; Hobbie, E. K.; Lacerda, S. H.; Migler, K. B.; Jakupciak, J. P. Length-dependent uptake of DNA-wrapped single-walled carbon nanotubes. *Adv. Mater.* **2007**, *19* (7), 939.

(35) Fagan, J. A.; Simpson, J. R.; Bauer, B. J.; Lacerda, S.; Becker, M. L.; Migler, K. B.; Hight Walker, A. R.; Hobbie, E. K. Length-Dependent Optical Effects in Single-Wall Carbon Nanotubes. *J. Am. Chem. Soc.* **2007**, *129*, 10607–10612.

(36) Bauer, B. J.; Becker, M. L.; Bajpai, V.; Fagan, J. A.; Hobbie, E. K.; Migler, K.; Guttman, C. M.; Blair, W. R. Measurement of single-wall nanotube dispersion by size exclusion chromatography. *J. Phys. Chem. C* **2007**, *111*, 17914–17918.

(37) Fagan, J. A.; Simpson, J. R.; Landi, B. J.; Richter, L. J.; Mandelbaum, I.; Bajpai, V.; Ho, D. L.; Raffaelle, R.; Walker, A. R. H.; Bauer, B. J.; Hobbie, E. K. Dielectric response of aligned semiconducting single-wall nanotubes. *Phys. Rev. Lett.* **2007**, *98*, 147402.

(38) Roe, R.-J. *Methods of X-ray and Neutron Scattering in Polymer Science*; Oxford University Press: New York, 2000.

(39) Hobbie, E. K. Optical anisotropy of nanotube suspensions. *J. Chem. Phys.* **2004**, *121* (2), 1029–1037.

(40) Jorio, A.; Santos, A. P.; Ribeiro, H. B.; Fantini, C.; Souza, M.; Vieira, J. P. M.; Furtado, C. A.; Jiang, J.; Saito, R.; Balzano, L.; Resasco, D. E.; Pimenta, M. A. Quantifying carbon-nanotube species with resonance Raman scattering. *Phys. Rev. B* **2005**, *72* (7).